

ANGULAR MOMENTUM EVOLUTION OF YOUNG STARS
IN THE NEARBY SCORPIUS-CENTAURUS OB ASSOCIATION

SAMUEL N. MELLON,^{1,2} ERIC E. MAMAJEK,^{3,1} THOMAS E. OBERST,² AND MARK J. PECAUT⁴

¹*Department of Physics & Astronomy, University of Rochester, Rochester, NY 14627, USA*

²*Department of Physics, Westminster College, New Wilmington, PA 16172, USA*

³*Jet Propulsion Laboratory, California Institute of Technology, M/S 321-100, 4800 Oak Grove Drive, Pasadena, CA 91109, USA*

⁴*Department of Physics, Rockhurst University, Kansas City, MO 64110, USA*

(Received; Revised; Accepted June 7, 2017)

Submitted to ApJ

ABSTRACT

We report the results of a study of archival SuperWASP light curves for stars in Scorpius-Centaurus (Sco-Cen), the nearest OB association. We use SuperWASP time-series photometry to extract rotation periods for 189 candidate members of the Sco-Cen complex, and verify that 162 of those are members of the classic Sco-Cen subgroups of Upper Scorpius (US), Upper Centaurus-Lupus (UCL), and Lower Centaurus-Crux (LCC). This study provides the first measurements of rotation periods explicitly for large samples of pre-main sequence (pre-MS) stars spanning the UCL and LCC subgroups. Our final sample of 157 well-characterized pre-MS stars spans ages of $\sim 10 - 20$ Myr, spectral types of $\sim F3 - M0$, and masses of $M \simeq 0.3 - 1.5 M_{\odot}^N$. For this sample, we find a distribution of stellar rotation periods with a median of $P_{\text{rot}} \simeq 2.4$ days, overall range of $0.2 < P_{\text{rot}} < 8$ days, and a fairly well-defined mass-dependent upper envelope of rotation periods. This distribution of periods is consistent with recently developed stellar angular momentum evolution models. These data are significant because they represent an undersampled age range and the number of measurable rotation periods is large compared to recent studies of other regions. We also search for new examples of eclipsing disk or ring systems analogous to 1SWASP J140747.93-394542.6 (“J1407”, V1400 Cen), but find none. Our survey yielded five eclipsing binaries, but only one appears to be physically associated with the Sco-Cen complex. V2394 Oph is a heavily reddened ($A_V \simeq 5$ mag) massive contact binary in the LDN 1689 cloud whose Gaia astrometry is clearly consistent with kinematic membership with the Ophiuchus star-forming region.

Keywords: open clusters and associations: individual (Lower Centaurus-Crux, Lupus, Ophiuchus, Upper Centaurus-Lupus, Upper Scorpius, Sco-Cen) — stars: binaries: eclipsing — stars: pre-main sequence — stars: rotation — stars: starspots

1. INTRODUCTION

The Scorpius-Centaurus OB Association (Sco-Cen) is the nearest OB association to the Sun ($d \simeq 118 - 145$ pc; de Zeeuw et al. 1999; Preibisch & Mamajek 2008). It contains the nearest *large* sample of 10 – 20 Myr stars, making it valuable for direct imaging of giant exoplanets and studies of disk evolution. The group is composed of three classically defined subgroups: Upper Scorpius (US; median age $\simeq 11$ Myr), Upper Centaurus-Lupus (UCL; median age $\simeq 16$ Myr), and Lower Centaurus-Crux (LCC; median age $\simeq 17$ Myr) (Pecaut et al. 2012; Pecaut & Mamajek 2016). This grouping can be problematic, however, as the boundaries of the subgroups are somewhat ill-defined and each group exhibits significant substructure (Preibisch & Mamajek 2008; Rizzuto et al. 2012; Pecaut & Mamajek 2016). Most stars located in the three subgroups with masses of $< 2 \mathcal{M}_{\odot}^{\text{N}1}$ are pre-main sequence (pre-MS), and some are still accreting from protoplanetary disks (e.g. Luhman & Mamajek 2012; Pecaut & Mamajek 2016). Throughout this paper, we refer to the collection of the classic subgroups US, UCL, and LCC as the Sco-Cen OB Association. We refer to the ensemble of active and recent star-formation in the vicinity of the Sco-Cen association as the *Sco-Cen complex*, including the young associations in the Oph, Lup, CrA, and Cha molecular clouds, and the smaller peripheral groups of $\sim 5 - 10$ Myr-old stars (ϵ Cha, η Cha, and TW Hya; Preibisch & Mamajek 2008). These regions represent a large-scale star-formation event that has been occurring over the past ~ 20 Myr, forming discrete subgroups of batches of dozens to thousands of stars during that span. The three classic subgroups likely represents ensembles of numerous smaller star-formation events rather than monolithic bursts of star formation (Pecaut & Mamajek 2016).

The distribution of rotation periods for pre-MS stars in Sco-Cen can provide useful constraints on stellar angular momentum evolution models. The angular momentum evolution of young stars is governed by several processes that work to increase or decrease the rotation speed of the star. During the pre-MS portion of a star’s lifetime the gravitational contraction lowers the star’s moment of inertia, which can increase the angular rotation speed as a consequence of angular momentum conservation; magnetic disk-locking can also work against this contraction (Irwin et al. 2011; Gallet & Bouvier 2013). Beyond the zero-age main sequence (ZAMS), the moment of inertia changes very slowly and the star’s

angular momentum evolution is dominated by braking via magnetized stellar winds and the transfer of angular momentum between the interior and exterior layers of the star causing a steady spin-down for the remainder of the star’s life (Gallet & Bouvier 2015).

In recent years, rotation periods have been measured for hundreds of stars over a wide range of masses (e.g. Hartman et al. 2008, 2010; Messina et al. 2010; Meibom et al. 2011a,b; Irwin et al. 2011; Gallet & Bouvier 2013; Moraux et al. 2013; Cargile et al. 2014; Meibom et al. 2015; Gallet & Bouvier 2015; Douglas et al. 2016). These distributions of rotation periods as a function of stellar age have enabled the development of angular momentum evolution models. These models, which are used to estimate the ages of stars from the earliest pre-MS through the end of the MS, take into account disk-locking, gravitational contraction, stellar winds, and many other factors (e.g. Meibom et al. 2011a; Barnes 2010; Reiners & Mohanty 2012; Bouvier et al. 2014; Cargile et al. 2014; Gallet & Bouvier 2015). Additional large surveys of rotation periods during the post-accretion pre-MS phase can help constrain these angular momentum evolution models as this age range is undersampled (e.g. Gallet & Bouvier 2015).

The work presented in this paper found rotation periods for 189 young stars, 96 of which are newly measured periods (including an outlying K giant star with a newly measured short activity period). 162 of these stars belong to the three classic subgroups (US, UCL, LCC). 157 of the Sco-Cen members had retrievable spectral types, which were used to estimate the masses of each star. The stars with spectral types were then plotted against current theoretical angular momentum evolution models from Gallet & Bouvier (2015). This study finds that these data are consistent with what these models predict.

This study was also designed to discover and characterize new circumsecondary eclipsing disk/ring systems like the one found around J1407 (V1400 Cen; Mamajek et al. 2012; Scott et al. 2014; Kenworthy & Mamajek 2015) and new examples of rare pre-MS eclipsing binary stars (e.g. Morales-Calderón et al. 2012; Kraus et al. 2015). No new eclipsing disk systems were discovered. Five candidate eclipsing binary systems were identified. However, upon further scrutiny, only *one* appears to be associated with Sco-Cen.

This paper is organized as follows: §2 discusses the construction of our initial sample of Sco-Cen candidates and details the data used in the survey; §3 details the use of periodograms and generation of phase-folded light curves; §4 provides a summary of the study’s results, discusses the rotational periods of the Sco-Cen members

¹ $\mathcal{M}_{\odot}^{\text{N}}$ is the symbol for the nominal solar mass as defined by IAU Resolution 2015 B3 (Prša et al. 2016).

and how these rotational periods help to understand the evolution of low-mass stars.

2. DATA

2.1. *Sco-Cen Sample & Membership*

In the course of previous work on the membership and star formation history of the Sco-Cen complex (including both the OB subgroups and related young stellar object populations in the associated molecular clouds; see e.g. [Preibisch & Mamajek 2008](#); [Pecaut et al. 2012](#); [Pecaut & Mamajek 2016](#)), an internal database was constructed of 5,551 candidate stellar members. For the classic subgroups, candidate members were drawn from the following studies: [Ardila et al. \(2000\)](#), [Blaauw \(1946\)](#), [Dawson et al. \(2011\)](#), [de Geus et al. \(1989\)](#), [Hoogerwerf et al. \(2000\)](#), [Lodieu et al. \(2006\)](#), [Lodieu et al. \(2007\)](#), [Lodieu et al. \(2013\)](#), [Luhman & Mamajek \(2012\)](#), [Mamajek et al. \(2002\)](#), [Martín et al. \(2004\)](#), [Pecaut et al. \(2012\)](#), [Pecaut & Mamajek \(2016\)](#), [Preibisch & Mamajek \(2008\)](#), [Rizzuto et al. \(2012\)](#), [Sartori et al. \(2003\)](#), [Slesnick et al. \(2006\)](#), [Song et al. \(2012\)](#), [Wichmann et al. \(1997\)](#), and [de Zeeuw et al. \(1999\)](#). The quality of membership assignments in these studies is quite heterogeneous. Some were selected only by virtue of photometry, proper motions, and/or X-ray emission. Many were also vetted using parallaxes and proper motions from the first Gaia data release ([Gaia Collaboration et al. 2016](#)). Given the large number of candidate members, memberships were only reassessed if a star passed several criteria summarized in §3.1.2.

2.2. *Photometry*

2.2.1. *SuperWASP Photometry*

In order to estimate both long-term median magnitudes and rotational periods (i.e. periodic variations in magnitudes due to starspot rotation) for Sco-Cen stars, these 5,551 candidate members were cross-referenced with the archival single-band time-series photometric data catalogue from the Super Wide Angle Search for Planets (SuperWASP). SuperWASP consists of two robotic observatories in La Palma, Spain, and Sutherland, South Africa. Each observatory has a bank of eight wide-angle cameras that collectively provide a 490 deg² field of view (FOV) per pointing at 13'' pix⁻¹ scale within magnitude range $8 < V < 13$. The observatories have been operating simultaneously and year-round since 2004 to collect *V*-band photometry over most of the sky with a single-position cadence of approximately 10 minutes ([Pollacco 2006](#); [Butters et al. 2010](#); [Smith & WASP Consortium 2014](#)).

The first and only SuperWASP public data release includes data collected between 2004 and 2008. It is avail-

able for download via the NASA Exoplanet Archive operated at the NASA Exoplanet Science Institute². The data were processed via the SuperWASP pipeline and post-pipeline analysis including astrometric calibration, aperture photometry, and photometric calibration. The data are provided in *.FITS and *.tbl formats, the latter containing observation timestamps (HJD), magnitudes calibrated to the Tycho-2 V_T system, and their uncertainties ([Pollacco 2006](#); [Butters et al. 2010](#)). SuperWASP fields in the Sco-Cen region were covered over three ~ 100 day seasons between 2006 and 2008. Of the 5,551 candidate Sco-Cen members, 1,689 of them were found to have SuperWASP counterparts.

A data reduction and periodogram analysis pipeline was used to process SuperWASP time series photometry (described in §3.1) for each of the 1,689 candidate stars. Table 1 contains the raw results from 1689 light curves, which includes the strongest periods (excluding obvious aliases) and fitted amplitudes for these periods from each season.

Only 189 of them were found to have rotation periods that were consistent throughout at least two of the 2006 – 2008 seasons. Of those 189 stars, 162 of them were confirmed as members of classic subgroups (plotted in Figure 1, see §2.2.2). Table 2 contains the reduced period and stellar information for these 162 stars. This sample is further trimmed to 157 stars for aspects of the analysis requiring spectral types since seven of the stars do not have a measured spectral type.

The remaining 27 stars belong to associated younger star-forming regions in the Sco-Cen complex, namely the Lup, Oph, and CrA regions (and two foreground members of the TW Hya association and a background Li-rich K giant). These 27 stars were not used in the subsequent analysis as their numbers are small (the effects of extinction are likely greatly reducing the coverage of members of these star-forming regions in SuperWASP catalog). These stars are compiled in Table 3 including their statistically significant periods.

2.2.2. *Multi-Band Photometry*

Due to the large pixel size of the SuperWASP survey (13.7'' pixel⁻¹), the median V_T magnitude may represent the unresolved light from multiple stars, which can result in spurious estimates of colors, reddening, and extinction (see §3.2). Thus, in addition to SuperWASP single-band time-series photometry, multi-band single instance (non-time-series) photometry from the archival databases of the Two Micron All-Sky Survey (2MASS; [Cutri et al. 2003b](#); [Skrutskie et al. 2006](#)), the fourth

² <http://exoplanetarchive.ipac.caltech.edu/>

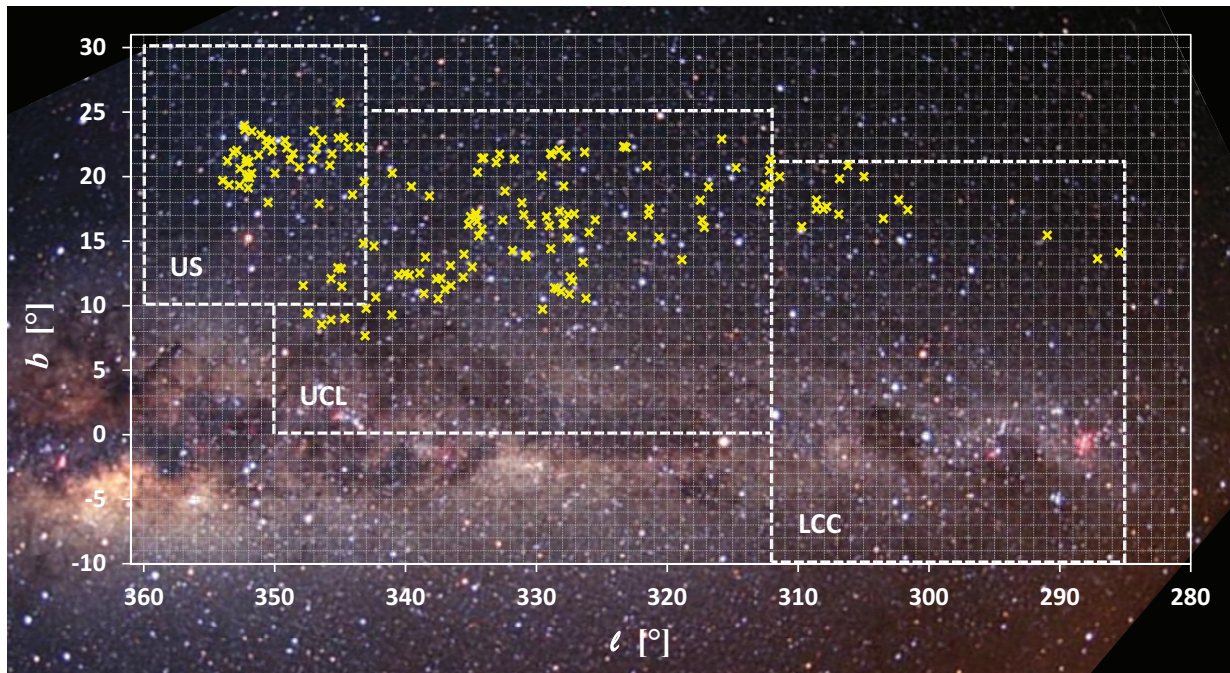


Figure 1. The distribution of Sco-Cen members with rotation periods plotted in Galactic Coordinates (yellow crosses). The background is a wide field optical image of the Sco-Cen region taken by Fred Espenak (NASA GSFC; www.mreclipse.com). The classic Sco-Cen subgroup boundaries defined by de Zeeuw et al. (1999) are plotted as dashed white lines.

United States Naval Observatory CCD Astrograph Catalog, (APASS; Henden et al. 2012), and the Yale/San Juan Southern Proper Motion Catalog 4 (SPM4; Girard et al. 2011) were used. These data were employed for three purposes: (1) to convert SuperWASP’s Tycho-2 V_T magnitudes to Johnson V_J magnitudes; (2) to help verify the membership of our Sco-Cen candidates; and (3) to obtain accurate V -band magnitudes for estimates of observed colors, estimated reddenings, and HR diagram placement for the target stars.

To convert SuperWASP’s Tycho-2 V_T magnitudes to the Johnson V_J system, two linear trends were fit to the Tycho-2 (Høg et al. 2000) and 2MASS (Skrutskie et al. 2006) photometry for nearby ($d < 75$ pc) *Hipparcos* stars whose absolute magnitudes were within 1 mag of the main sequence, and whose photometric errors were < 0.03 mag in the relevant bands:

$$V_J - V_T = -0.095 - 0.062(V_T - J - 1.631) \quad (1)$$

$$V_J - V_T = -0.083 - 0.049(V_T - H - 1.791) \quad (2)$$

The uncertainties in the zero-points are 0.001 mag, and uncertainties in the slopes are 0.002, while the rms dispersions in the fits are 0.01 mag. The fits are well-constrained over the color ranges $0 < (V_T - J) < 3.6$ and $0 < (V_T - H) < 4.2$.

While cross-referencing the SuperWASP and 2MASS data, we found that, for approximately one-third of the stars in our sample, the best spatial matches had poor brightness matches. The worst offenders revealed themselves as unphysical outliers on a color-magnitude diagram (V_J vs. $V_{\text{APASS}} - K_s$). These cases were found to each be caused by two 2MASS targets of significant ($\gtrsim 0.75$ magnitude) brightness difference existing in close spatial proximity to a single SuperWASP target. Each was corrected by simply selecting the 2MASS counterpart as the one of (obvious) comparable brightness to the SuperWASP target.

Many smaller but significant ($0.2 \lesssim \Delta V \lesssim 0.75$ magnitudes) brightness differences remained in cases with no spatial degeneracy of 2MASS counterparts. This prompted us to compare the SuperWASP and 2MASS brightnesses and positions with those of the APASS and SPM4 surveys as an additional check. The 2MASS, APASS, and SPM4 brightnesses were found to be in excellent agreement: e.g. $(\Delta V)_{\text{average}} \simeq 0.01$ magnitudes for the APASS and SPM4 catalogs. However, the SuperWASP brightnesses were found to have much poorer agreement: e.g. $(\Delta V)_{\text{average}} \simeq 0.1$ mag when comparing the converted SuperWASP V magnitudes to either of the APASS or SPM4 catalogs, a factor of 10 worse. Figure 2 panel (a) shows the distribution of brightness differences between SuperWASP and APASS. The sizable skewing of SuperWASP data to brighter magnitudes can be at-

tributed to blending due to SuperWASP’s large pixel scale. Panels (b), (c) and (d) show the J2000 positional differences between the four surveys. While these differences are all small at $(\Delta r)_{\text{average}} < 0.6''$ or better, the APASS positions agree best with those of 2MASS at $(\Delta r)_{\text{average}} = 0.12''$.

APASS Johnson V -band magnitudes were used instead of the converted SuperWASP V magnitudes for all other aspects of our study (e.g. colors, reddening, HR diagram analysis). All of this gave us the highest confidence in the APASS V magnitudes and the lowest confidence in the SuperWASP V magnitudes. SPM4 Johnson V magnitudes were adopted only for the five stars in our 162-star sample for which APASS V magnitudes are not available. Finally, we computed $V - K_s$ colors for the stars in our sample using the adopted V magnitudes (from APASS or SPM4) and 2MASS K_s magnitudes. Figure 3 shows a de-reddened color-magnitude diagram for the final sample of 162 members of the three Sco-Cen subgroups. The treatment used for interstellar reddening and extinction is discussed later in §3.2.

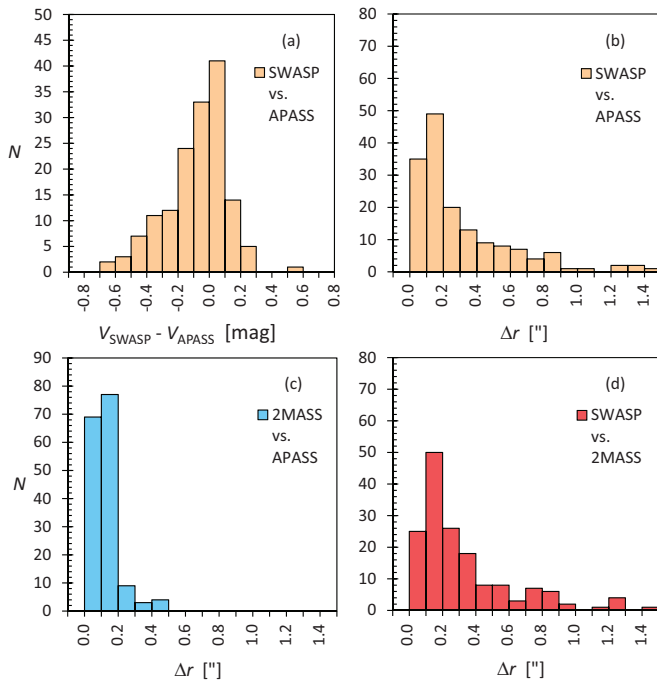


Figure 2. Select distributions of spatial and brightness differences between the SuperWASP, APASS, and 2MASS data sets for the final 162 star sample. In Panel (a) the brightnesses for both surveys are in Johnson V magnitudes. The remaining panels show the J2000 positional differences.

3. ANALYSIS

3.1. Time-Series Analysis

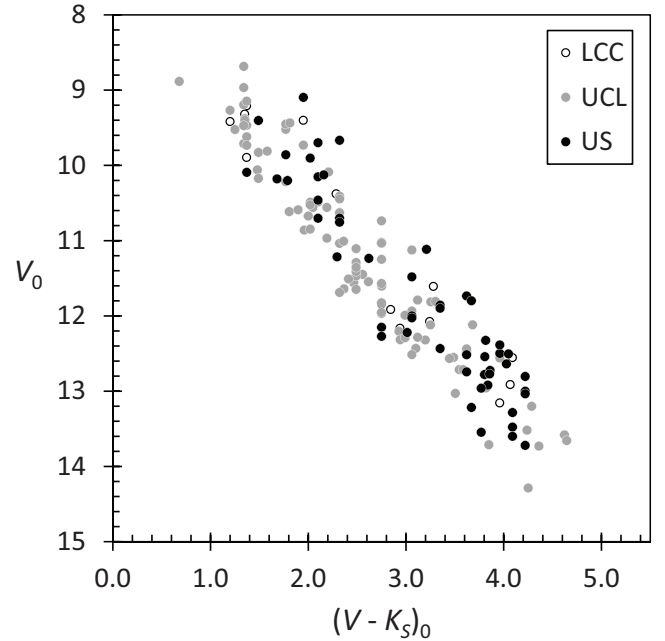


Figure 3. De-reddened color-magnitude diagram for the final sample of 162 stars in the classic Sco-Cen subgroups of US (filled black circles), UCL (filled gray circles), and LCC (open circles). The V -band brightness on both axes is APASS Johnson V , and the K_s value is from 2MASS.

3.1.1. Data Reduction

SuperWASP photometric data requires additional data reduction beyond its own pipelines (Collier Cameron et al. 2006). Reported photometric errors, median binning, and a 3σ clip were used to further reduce the data. Data points with reported photometric errors of > 0.1 mag were removed. Each data set was median combined and the standard error of the mean for each binned point was recorded; the low-period limit of 0.1 days was used because stars are not expected to have rotation periods shorter than this due to instability (Hartman et al. 2010). Bins with fewer than 3 points were removed. A 3σ clip was applied to the binned data to remove any remaining spurious points. The reduced data was separated into three individual ~ 100 day time frames (seasons). Finally, a plot of the full light curve, with error bars, was generated (Figure 4).

3.1.2. Periodograms

A custom periodogram analysis pipeline was written using the Python³ language. Modules from the SciPy⁴ stack: `scipy`, `numpy`, `matplotlib`, and `pandas` (Jones

³ <http://python.org>

⁴ <http://www.scipy.org/>

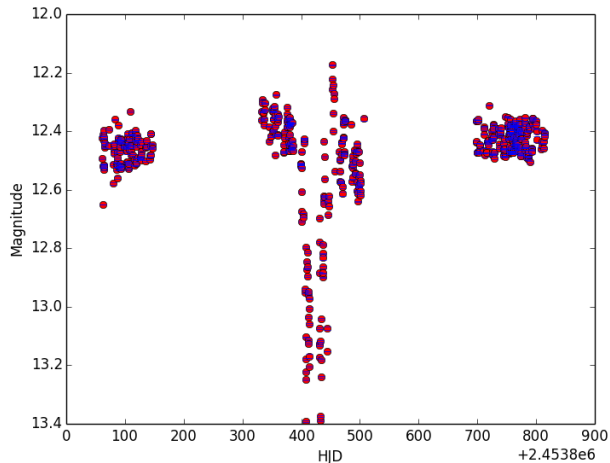


Figure 4. The reduced SuperWASP light curve for V1400 Cen (‘‘J1407’’) over three observing seasons. Error bars (blue) are smaller than the data points themselves. The transit reported in Mamajek et al. (2012) is clearly detected.

et al. 2001–; Stfan van der Walt & Varoquaux 2011; Hunter 2007; McKinney 2010) were used for reducing and plotting data (with error bars) (§3.1.1), performing Lomb-Scargle periodograms, and generating phase-folded light curves with fitted amplitudes.

The Lomb-Scargle (LS) periodogram (Press et al. 1992; Scargle 1982) is a powerful tool for extracting periods from unevenly sampled time series photometry data sets (e.g. Hartman et al. 2008, 2010; Messina et al. 2010). The LS periodogram routine from the Python *scipy* module was applied to each observing season for each star. The period range spans from 0.1 days (see §3.1.1) to τ days with a period step size of 0.15 days where τ is half the length of time for the data collected in a particular season. Periods corresponding to half the time length of the data set (τ) were searched to ensure that all possible long term periods in the data set can be detected. The period stepsize provided a resolution in the periodogram fine enough to detect strong periods accurately over a large period span without being overly computationally expensive. After sorting data points into their individual seasons, the routine returned the normalized values, which were then plotted versus frequency.

We report the strongest period from each stars periodogram in Table 1. The LS periodogram routine alone does not estimate false positive periods, so the method of Cargile et al. (2014) was employed to calculate false alarm probabilities (FAPs). In the interest of computational time, FAPs were only calculated for our final 162

star sample (Table 2) and the 27 ‘‘other’’ stars (Table 3).

In short, the FAP for a given star was estimated by randomly shuffling its light curves photometric values relative to its time values (after binning), creating a new, randomized light curve. Next, a periodogram was created for this randomized light curve and its strongest period saved. This was repeated 10^4 times, and the resulting strongest periods were plotted as a histogram. Finally, the strongest period from the *real* light curve was compared to this histogram. The period was considered to be a real detection only if less than 10% of the histograms periods had stronger peaks. In this case we say the the FAP < 0.01 . Obvious aliases (periods occurring at integer multiples of the strongest period) were vetted by eye. Figure 5 shows three example light curves with their corresponding periodograms and FAP levels.

Uncertainties for the periods were measured only for the stars presented in Table 2 and Table 3. The maximum peak in the periodogram for each season was fit with a Gaussian using a least-squares routine. The means and variances were averaged for each season and reported in Table 2 and Table 3. The light curves for each star was then phase-folded over its seasonal period and plotted. Using the *scipy* least-squares fitting tool, a sine curve is fit to each phase-folded light curve (Figure 5).

Figure 5 contains example periodograms and light curves for three example stars in our sample. The criteria for a detected rotation period are (1) a periodogram peak must be above the 0.01 FAP plot threshold, (2) that said peak is consistent through *at least two* seasons of SuperWASP data, and (3) a consistent light curve amplitude (to within a few 0.1 magnitudes) through at least two seasons. Further, the stars reported must be confirmed members of Sco-Cen (see §2.2.1). In order to completely profile each star and compare them onto angular momentum evolution models (see Figures 7 & 8), the star must have a published spectral type and be a member of one of the three main subgroups.

3.2. Intrinsic Color, Temperature, and Mass Modeling

To investigate the angular momentum evolution of Sco-Cen stars, it is constructive to plot the rotation periods determined from the periodogram analysis as a function of intrinsic stellar properties. In particular, the measured spectral types for 157 stars in our sample enabled us to estimate intrinsic colors ($V - K_s$), effective temperatures (T_{eff}), and masses (M). The intrinsic $V - K_s$ and T_{eff} were determined from the empirical relations and BT-Settl grid models, respectively, from Ta-

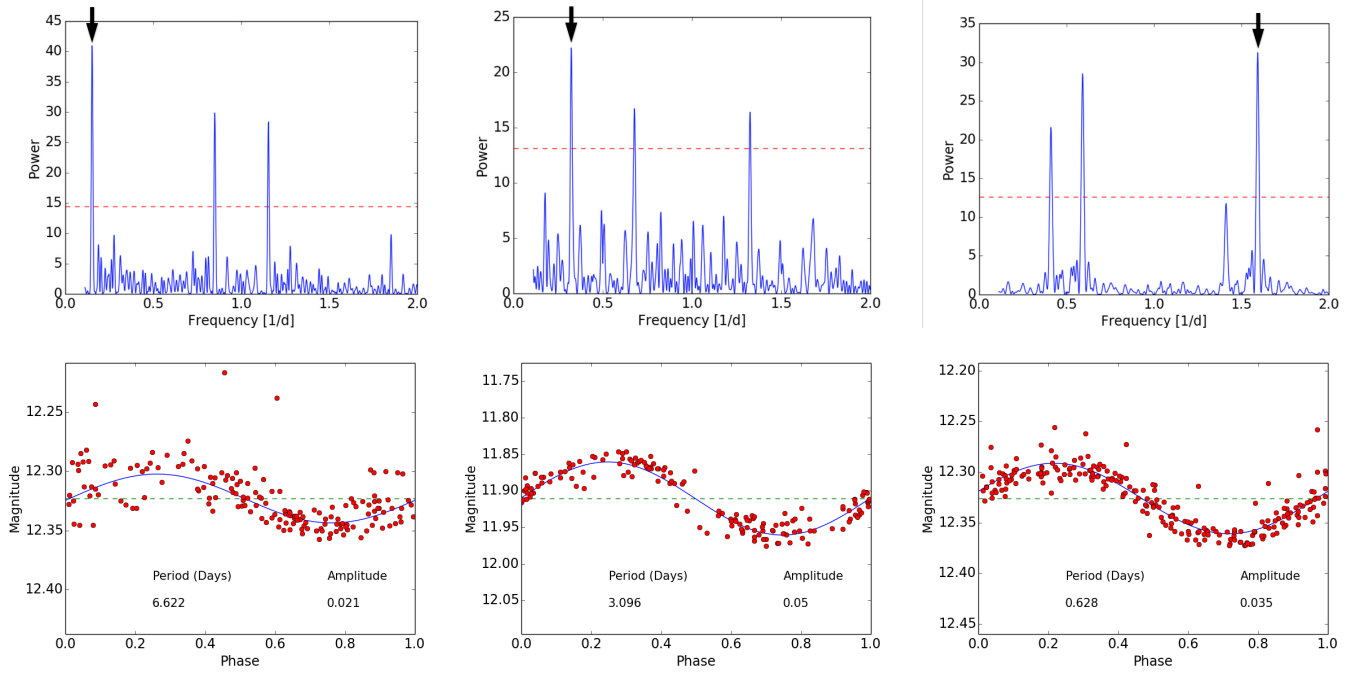


Figure 5. Periodograms (top figures) and phase-folded light curves (bottom figures) for three stars, illustrating a range of periods and amplitudes. The dashed red line represents the power at the 0.01 FAP and the adopted frequencies for each star are marked with a black arrow. In the light curves, best-fit sinusoid is plotted in blue and the green dashed line represents the SWASP mean magnitude. *Left:* 2MASS J15082502-3337554, *Center:* 2MASS J13191370-4506326, *Right:* 2MASS J11132622-4523427.

ble 6 of Pecaut & Mamajek (2013). Based on these T_{eff} values, we computed M using the theoretical isochrones of (Baraffe et al. 2015, hereafter BHAC15) (adopting the mean age of each star’s subgroup):

$$\begin{aligned} \log(M/M_{\odot}^{\text{N}}) = & -(3.5075918704 \times 10^4) \\ & + (3.7421144677 \times 10^4) \cdot \log(T_{\text{eff}}) \\ & - (1.4972186556 \times 10^4) \cdot \log(T_{\text{eff}})^2 \\ & + (2.6625089056 \times 10^3) \cdot \log(T_{\text{eff}})^3 \\ & - (1.7755725859 \times 10^2) \cdot \log(T_{\text{eff}})^4, \end{aligned} \quad (3)$$

this is valid over the range $3056 \text{ K} < T_{\text{eff}} < 6422 \text{ K}$ and $0.1 < M/M_{\odot}^{\text{N}} < 1.4$, and has a calibration uncertainty of approximately $\sigma(\log(M/M_{\odot}^{\text{N}})) \simeq 0.007$ dex. Table 2 lists the intrinsic $V - K_s$, T_{eff} , and masses determined for the stars in our sample, and period-color, period-temperature, and period-mass diagrams are plotted in Figure 6.

Interstellar reddening was estimated using $B - V$, $V - J$, $V - H$, and $V - K_s$. The observed colors were computed from BV photometry collected from various sources (e.g., APASS DR9, Hipparcos, Tycho-2, or other ground-based photometry) and near-infrared photometry from 2MASS (Cutri et al. 2003a). The photometry adopted for estimating extinctions is listed in Table 4. The observed photometry was then compared to intrinsic color sequences for pre-MS stars as a function of spectral type from Pecaut & Mamajek (2013) to estimate color excesses $E(B - V)$, $E(V - J)$, $E(V - H)$, and $E(V - K_s)$. Extinctions for individual objects were computed using these four color excesses, as described in Pecaut & Mamajek (2016). The computed extinctions for each star are listed in Table 2.

For stars without a measured spectral type, the color excess and extinction coefficient were taken as the average of the other stars in the same subgroup: $E(V - K_s)_{\text{avg}} = 0.332$ for US and 0.173 for each of UCL and LCC; $(A_V)_{\text{avg}} = 0.372$ for US and 0.194 for each of UCL and LCC. These mean color excesses and extinctions were used to correct the observed V and $V - K_s$ values in the color-magnitude diagram of Figure 3 and the observed $V - K_s$ colors in the period-color plot of Figure 6 Panel (a).

4. DISCUSSION

4.1. Results

Table 2 summarizes the relevant stellar parameters for our sample stars, including SWASP – 2MASS cross-identifications, Sco-Cen sub-group assignments, season-averaged rotation periods, spectral types, colors, extinctions, effective temperatures, and estimated masses. A

search of the literature found only one variability study of stars across Sco-Cen with which to compare (David et al. 2014). We find that the only star with a reported period in both our survey and David et al. (2014) was HD 141277 (2MASS J15494499-3925089), with both surveys reporting the same rotation period of ~ 2.23 days. We queried the AAVSO International Variable Star Index (VSX) catalog via VizieR using the 2MASS positions of our stars, with a $5''$ search radius; the search uncovered the nearest spatial matches (most $< 1''$ away) for 94 of our stars (Watson 2006). Of these 94 stars, 76 have periods similar to ours. There are 96 new rotation period measurements, including a second, shorter activity period measured for the Li-rich K giant CD-43 6891.

4.2. Rotational Evolution

For each star, we adopt the mean age of its subgroup and use its spectral type (and corresponding T_{eff}) to estimate a mass using isochrones (see §3.2). Figure 7 is a mass-period diagram for Sco-Cen with rotational evolution tracks from Gallet & Bouvier (2015) overplotted for several rotation rates at the ages of each major subgroup. In addition, a quadratic is plotted in an attempt visualize the rotational evolution trend of the ~ 11 -17 Myr sample of pre-MS stars. The season-averaged rotation periods versus the age of each subgroup are plotted in Figure 8. The Gallet & Bouvier (2015) rotational evolution tracks are overplotted for different stellar masses and initial conditions (fast, medium, slow rotators); initial conditions were chosen to best match rotation period distributions of older and younger clusters. Our data show that the general trend in period and mass predicted by the Gallet & Bouvier (2015) models continue to do a reasonable job matching the Sco-Cen stars. The envelope of the fastest rotators in Sco-Cen between $\sim 0.5 - 1 M_{\odot}^{\text{N}}$ follows the fast rotator trend predicted by Gallet & Bouvier (2015). We show a few stars with periods of ~ 8 days that are rotating slightly slower than the envelope of the slowest rotators predicted by the Gallet & Bouvier (2015) models. All of our $\sim 1.25 - 1.5 M_{\odot}^{\text{N}}$ stars are rotating very fast (0.2 – 3 days) and just below $\sim 1.25 M_{\odot}^{\text{N}}$ stars are found with much slower rotation periods of $\sim 5 - 6$ days.

These results suggests that while the stars that will eventually be early F dwarfs on the main sequence (F1V-F6V; $1.25 - 1.5 M_{\odot}^{\text{N}}$) have rotation periods at $\sim 11 - 17$ Myr that on average are only slightly less than their G-type brethren (~ 2 days vs. ~ 3 days, on average), the F dwarf population appears to arrive on the main sequence with a population near breakup velocity ($P \simeq 0.2$ day; e.g. 1SWASP J154610.69-384630.2, 1SWASP J144619.03-354146.5), but lacking a population of slow

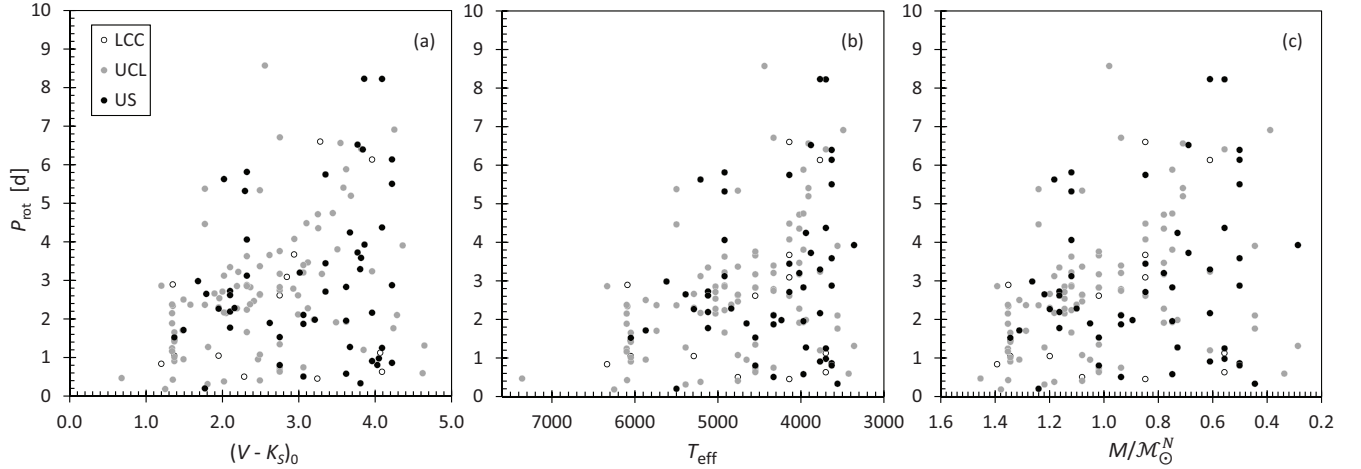


Figure 6. Period-color, -temperature, and -mass diagrams. The vertical axes plot the season-averaged rotation period determined from the SuperWASP periodogram analysis in units of days, P_{rot} . The horizontal axes plot the extinction-corrected observed color $V - K_s$ in magnitudes (Panel a), the modeled effective temperature T_{eff} in units of K (Panel b), and the modeled mass in units of solar masses, M/M_{\odot}^N (Panel c). Panel (a) contains the complete final sample of 162 stars in the classic Sco-Cen subgroups of US (filled black circles), UCL (filled gray circles), and LCC (open circles), whereas panels (b) and (c) contain only the 157 of these stars with measured spectral-types — since the temperature and mass models depend on the spectral type.

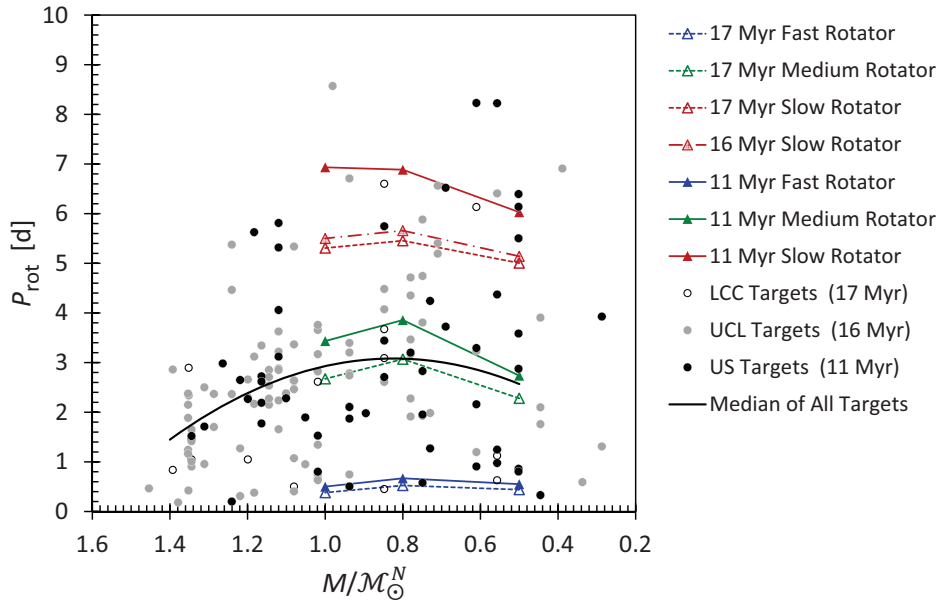


Figure 7. The period-mass diagram of Figure 6 panel (c) overlaid with the angular momentum evolutionary model tracks of Gallet & Bouvier (2015). As in Gallet & Bouvier (2015), tracks are shown for each of “slow,” “medium,” and “fast,” rotators corresponding to the 25th, 50th, and 90th percentiles in rotational period of the stellar envelope. The modeled points (triangles) have been averaged by mass in bins of 0.4 - 0.6, 0.7 - 0.9, and 0.9 - 1.1 M_{\odot}^N and are plotted at the mass bin centers; the connecting lines serve only to interpolate between these modeled points and do not themselves represent model data. Here only model tracks corresponding to the median ages of US, UCL, and LCC of 11, 16, and 17 Myr, respectively, are reproduced. Model tracks for the 16 Myr medium and fast rotators have been omitted since they are nearly identical to (i.e. overlap) those of the 17 Myr medium and fast rotators, respectively. For general comparison to the model tracks, a second-order polynomial (black solid line) was fit to the median periods of the 157 stellar data points (circles) in same three mass bins as the models plus two additional bins of 1.1 - 1.3 and 1.3 - 1.5 M_{\odot}^N .

rotators ($P > 3$ days). The early F-type stars remain fast-rotating throughout their main sequence lifetimes, experiencing only weak magnetic braking due to their weaker magnetic dynamos (e.g. Slettebak 1955; Kraft 1967).

4.3. Search for Eclipsing Systems

In addition to our rotation evolution study, this analysis included a search for any signatures of circumsecondary disks similar to 1SWASP J140747.93-394542.6 (“J1407” = V1400 Cen; Mamajek et al. 2012; Scott et al. 2014). The asymmetric light curves of the stars ϵ Aurigae (Guinan & Dewarf 2002), EE Cep (Mikolajewski & Graczyk 1999), and J1407 are signatures of disk or ring systems occulting their host stars. These asymmetric eclipses are characterized by their long duration and magnitude-scale depths (e.g. EE Cep with a ~ 30 –90 day eclipse and depth of > 2 mag; Mikolajewski & Graczyk 1999). An effective large scale search for these eclipses (as proposed by Mamajek et al. 2012) would require a long term (10 year), high cadence time-series photometric survey of 10^4 post-accretion pre-MS stars — yielding only a few candidates.

All of the light curves from this analysis were scanned by eye for obvious eclipses like J1407 (see Figure 4). To see an eclipse occur, it would have to be restricted to one of these 100 day windows (J1407 has a ~ 58 day eclipse duration; Mamajek et al. 2012). Additionally, the rotation period amplitudes vary on the 0.01 magnitude level (see Table 1). Thus, any amplitude variations on the 0.1 magnitude level would be evident in our periodogram search, making shorter term < 10 day eclipses evident. Therefore, no eclipses with durations of < 100 days and depths > 0.1 magnitudes were detected in this sample.

This survey also uncovered five candidates for pre-MS eclipsing binaries. However, after further review of their astrometric data, we reject Sco-Cen membership for four of them. We argue that one of them (V2394 Oph) appears to be a poorly characterized, heavily reddened ($A_V \simeq 5$ mag) massive eclipsing binary in the LDN 1689 dark cloud of the Ophiuchus star-forming region of Sco-Cen. Further discussion on these eclipsing binaries can be found in the Appendix.

4.4. Conclusion

This survey searched the SuperWASP archive for Sco-Cen members with measurable rotation periods and significant eclipsing events. A total of 189 reliable rotation periods were extracted – 162 for stars in the classic Sco-Cen subgroups of US, UCL, and LCC, and 27 for stars in younger star-forming regions within the Sco-Cen complex. Of these, 157 of the classic subgroup members have previously reported spectral types. These spectral types were used to estimate masses to compare our data against current angular momentum evolution models from Gallet & Bouvier (2015), and the rotation periods appear to be in reasonable agreement with the range of periods predicted by the models. No new eclipsing circumsecondary disks were detected beyond the previously known V1400 Cen (J1407) system. Five eclipsing binary systems were identified, but only one appears to be a strong candidate for membership in Sco-Cen (V2394 Oph in the LDN 1689 dark cloud in Ophiuchus). The remaining four eclipsing binaries all appear to be interlopers.

ACKNOWLEDGEMENTS

SNM was supported by NSF award PHY-1156339 for the University of Rochester REU program. EEM acknowledges support from NSF award AST-1313029. SNM and EEM also acknowledge support from the NASA NExSS program. This work used the VizieR and SIMBAD services. Part of this research was carried out at the Jet Propulsion Laboratory, California Institute of Technology, under a contract with the National Aeronautics and Space Administration. We also acknowledge and thank Florian Gallet for providing the angular momentum evolution tracks used to generate Figures 7 & 8. This paper makes use of data from the first public release of the WASP data (Butters et al. 2010) as provided by the WASP consortium and services at the NASA Exoplanet Archive, which is operated by the California Institute of Technology, under contract with the National Aeronautics and Space Administration under the Exoplanet Exploration Program. This document has been approved for unlimited release (CL#17-2577).

REFERENCES

- Aller, L. H., Appenzeller, I., Baschek, B., et al., eds. 1982, Landolt-Börnstein: Numerical Data and Functional Relationships in Science and Technology - New Series ” Gruppe/Group 6 Astronomy and Astrophysics ” Volume 2 Schaifers/Voigt: Astronomy and Astrophysics / Astronomie und Astrophysik ” Stars and Star Clusters / Sterne und Sternhaufen, 54
- Antoniucci, S., García López, R., Nisini, B., et al. 2014, A&A, 572, A62
- Ardila, D., Martín, E., & Basri, G. 2000, AJ, 120, 479
- Baraffe, I., Homeier, D., Allard, F., & Chabrier, G. 2015, A&A, 577, A42

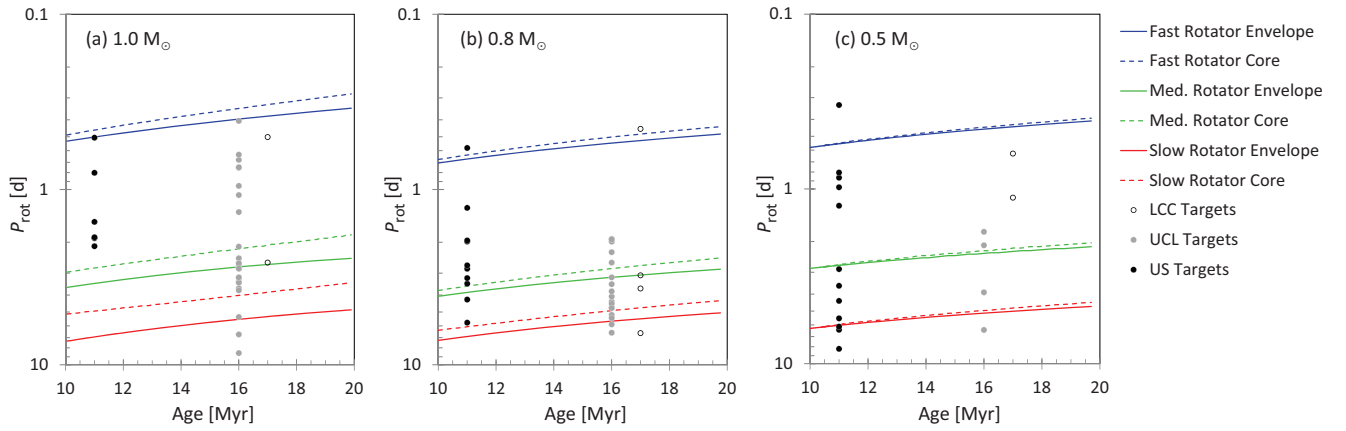


Figure 8. A reproduction of the period-age diagrams of Gallet & Bouvier (2015), Figure 5, with Sco-Cen stars from the present study (circles) overplotted. As in Gallet & Bouvier (2015), angular momentum evolutionary model tracks are shown for each of “slow,” “medium,” and “fast,” rotators corresponding to the 25th, 50th, and 90th percentiles in rotational period for each of the stellar core and envelope. The modeled data are also averaged by mass in bins of $0.4 - 0.6 M_{\odot}^{\text{N}}$ (panel a), $0.7 - 0.9 M_{\odot}^{\text{N}}$ (panel b), and $0.9 - 1.1 M_{\odot}^{\text{N}}$ (panel c). Only 82 of the final 162 star sample are shown since five do not have mass determinations and the rest have masses falling outside of these three mass ranges.

- Barnard, E. E. 1910, *ApJ*, 31, doi:10.1086/141719
- Barnes, S. A. 2010, *ApJ*, 722, 222
- Blaauw, A. 1946, *Publications of the Kapteyn Astronomical Laboratory Groningen*, 52, 1
- Bouvier, J., Matt, S. P., Mohanty, S., et al. 2014, *Protostars and Planets VI*, 433
- Butters, O. W., West, R. G., Anderson, D. R., et al. 2010, *A&A*, 520, L10
- Cargile, P. A., James, D. J., Pepper, J., et al. 2014, *ApJ*, 782, 29
- Chen, C. H., Mamajek, E. E., Bitner, M. A., et al. 2011, *ApJ*, 738, 122
- Collier Cameron, A., Pollaco, D., Street, R. A., et al. 2006, *MNRAS*, 373, 799
- Cutri, R. M., Skrutskie, M. F., van Dyk, S., & et al. 2003a, 2MASS Point Source Catalogue (available at <http://www.ipac.caltech.edu/2mass/>)
- Cutri, R. M., Skrutskie, M. F., van Dyk, S., et al. 2003b, *VizieR Online Data Catalog*, 2246, 0
- David, M., Hensberge, H., & Nitschelm, C. 2014, *Journal of Astronomical Data*, 20, 1
- Dawson, P., Scholz, A., & Ray, T. P. 2011, *MNRAS*, 418, 1231
- de Geus, E. J., de Zeeuw, P. T., & Lub, J. 1989, *A&A*, 216, 44
- de Zeeuw, P. T., Hoogerwerf, R., de Bruijne, J. H. J., Brown, A. G. A., & Blaauw, A. 1999, *AJ*, 117, 354
- Douglas, S. T., Agüeros, M. A., Covey, K. R., et al. 2016, *ApJ*, 822, 47
- Erickson, K. L., Wilking, B. A., Meyer, M. R., Robinson, J. G., & Stephenson, L. N. 2011, *AJ*, 142, 140
- Gaia Collaboration, Prusti, T., de Bruijne, J. H. J., et al. 2016, *A&A*, 595, A1
- Gallet, F., & Bouvier, J. 2013, *A&A*, 556, A36
- . 2015, *A&A*, 577, A98
- Girard, T. M., van Altena, W. F., Zacharias, N., et al. 2011, *AJ*, 142, 15
- Gontcharov, G. A. 2008, *Astronomy Letters*, 34, 785
- Grankin, K. N., Zakirov, M. M., Arzumanyants, G. C., & Melnikov, S. Y. 1996, *Information Bulletin on Variable Stars*, 4405
- Guinan, E. F., & Dewarf, L. E. 2002, in *Astronomical Society of the Pacific Conference Series*, Vol. 279, *Exotic Stars as Challenges to Evolution*, ed. C. A. Tout & W. van Hamme, 121
- Hartman, J. D., Bakos, G. Á., Kovács, G., & Noyes, R. W. 2010, *MNRAS*, 408, 475
- Hartman, J. D., Gaudi, B. S., Holman, M. J., et al. 2008, *ApJ*, 675, 1254
- Henden, A. A., Levine, S. E., Terrell, D., Smith, T. C., & Welch, D. 2012, *Journal of the American Association of Variable Star Observers (JAAVSO)*, 40, 430
- Henden, A. A., Templeton, M., Terrell, D., et al. 2016, *VizieR Online Data Catalog*, 2336
- Høg, E., Fabricius, C., Makarov, V. V., et al. 2000, *A&A*, 355, L27
- Hoogerwerf, R., de Bruijne, J. H. J., & de Zeeuw, P. T. 2000, *ApJL*, 544, L133
- Houk, N. 1978, *Michigan Catalogue of Two-dimensional Spectral Types for the HD stars. Volume 2, Declinations -53°.0 to -40°.0*.
- . 1982, *Michigan Catalogue of Two-dimensional Spectral Types for the HD stars. Volume 3, Declinations -40°.0 to -26°.0*.
- Houk, N., & Smith-Moore, M. 1988, *Michigan Catalogue of Two-dimensional Spectral Types for the HD Stars. Volume 4, Declinations -26°.0 to -12°.0*.
- Hughes, J., Hartigan, P., Krautter, J., & Kelemen, J. 1994, *AJ*, 108, 1071
- Hunter, J. D. 2007, *Matplotlib: A 2D Graphics Environment*, . <http://www.scipy.org/>
- Irwin, J., Berta, Z. K., Burke, C. J., et al. 2011, *ApJ*, 727, 56
- Jones, E., Oliphant, T., Peterson, P., et al. 2001–, *SciPy: Open source scientific tools for Python*, . <http://www.scipy.org/>
- Kenworthy, M. A., & Mamajek, E. E. 2015, *ApJ*, 800, 126
- Köhler, R., Kunkel, M., Leinert, C., & Zinnecker, H. 2000, *A&A*, 356, 541
- Kraft, R. P. 1967, *ApJ*, 150, 551
- Kraus, A. L., Cody, A. M., Covey, K. R., et al. 2015, *ApJ*, 807, 3
- Krautter, J., Wichmann, R., Schmitt, J. H. M. M., et al. 1997, *A&AS*, 123, 329
- Lodieu, N., Dobbie, P. D., Cross, N. J. G., et al. 2013, *MNRAS*, 435, 2474
- Lodieu, N., Hambly, N. C., & Jameson, R. F. 2006, *MNRAS*, 373, 95
- Lodieu, N., Hambly, N. C., Jameson, R. F., et al. 2007, *MNRAS*, 374, 372
- Loinard, L., Torres, R. M., Mioduszewski, A. J., & Rodríguez, L. F. 2008, *ApJL*, 675, L29
- Lombardi, M., Lada, C. J., & Alves, J. 2008, *A&A*, 480, 785
- Luhman, K. L., & Mamajek, E. E. 2012, *ApJ*, 758, 31
- Makarov, V. V. 2007, *ApJS*, 169, 105
- Mamajek, E. E. 2008, *Astronomische Nachrichten*, 329, 10
- Mamajek, E. E., & Hillenbrand, L. A. 2008, *ApJ*, 687, 1264
- Mamajek, E. E., Meyer, M. R., & Liebert, J. 2002, *AJ*, 124, 1670

- Mamajek, E. E., Quillen, A. C., Pecaú, M. J., et al. 2012, *AJ*, 143, 72
- Martín, E. L., Delfosse, X., & Guieu, S. 2004, *AJ*, 127, 449
- McKinney, W. 2010, *Data Structures for Statistical Computing in Python*, . <http://www.scipy.org/>
- Meibom, S., Barnes, S. A., Platais, I., et al. 2015, *Nature*, 517, 589
- Meibom, S., Mathieu, R. D., Stassun, K. G., Liebesny, P., & Saar, S. H. 2011a, *ApJ*, 733, 115
- Meibom, S., Barnes, S. A., Latham, D. W., et al. 2011b, *ApJL*, 733, L9
- Messina, S., Desidera, S., Turatto, M., Lanzafame, A. C., & Guinan, E. F. 2010, *A&A*, 520, A15
- Meyer, M. R., & Wilking, B. A. 2009, *PASP*, 121, 350
- Mikolajewski, M., & Graczyk, D. 1999, *MNRAS*, 303, 521
- Morales-Calderón, M., Stauffer, J. R., Stassun, K. G., et al. 2012, *ApJ*, 753, 149
- Moraux, E., Artemenko, S., Bouvier, J., et al. 2013, *A&A*, 560, A13
- Nutter, D., Ward-Thompson, D., & André, P. 2006, *MNRAS*, 368, 1833
- Ortiz-León, G. N., Loinard, L., Kounkel, M. A., et al. 2016, *ArXiv e-prints*, arXiv:1611.06466
- Pecaú, M. J., & Mamajek, E. E. 2013, *ApJS*, 208, 9
- . 2016, *MNRAS*, 461, 794
- Pecaú, M. J., Mamajek, E. E., & Bubar, E. J. 2012, *ApJ*, 746, 154
- Perevozkina, E. L., & Svechnikov, M. A. 2004, *VizieR Online Data Catalog*, 5118
- Perryman, M. A. C., Lindegren, L., Kovalevsky, J., et al. 1997, *A&A*, 323, L49
- Pollacco, D. L., e. a. 2006, *PASP*, 118, 1407
- Preibisch, T., Guenther, E., Zinnecker, H., et al. 1998, *A&A*, 333, 619
- Preibisch, T., & Mamajek, E. 2008, in *Handbook of Star Forming Regions, Volume II: The Southern Sky – ASP Monograph Publications, Vol. 5.*, ed. B. Reipurth, 235
- Press, W. H., Teukolsky, S. A., Vetterling, W. T., & Flannery, B. P. 1992, *Numerical recipes in FORTRAN. The art of scientific computing*
- Prša, A., Harmanec, P., Torres, G., et al. 2016, *AJ*, 152, 41
- Reiners, A., & Mohanty, S. 2012, *The Astrophysical Journal*, 746, 43.
<http://stacks.iop.org/0004-637X/746/i=1/a=43>
- Riaz, B., Gizis, J. E., & Harvin, J. 2006, *AJ*, 132, 866
- Richards, J. W., Starr, D. L., Miller, A. A., et al. 2012, *ApJS*, 203, 32
- Rizzuto, A. C., Ireland, M. J., & Kraus, A. L. 2015, *MNRAS*, 448, 2737
- Rizzuto, A. C., Ireland, M. J., & Zucker, D. B. 2012, *MNRAS*, 421, L97
- Rybka, S. P. 2007, *Kinematika i Fizika Nebesnykh Tel*, 23, 102
- Sartori, M. J., Lépine, J. R. D., & Dias, W. S. 2003, *A&A*, 404, 913
- Scargle, J. D. 1982, *ApJ*, 263, 835
- Scott, E. L., Mamajek, E. E., Pecaú, M. J., et al. 2014, *ApJ*, 797, 6
- Siess, L., Dufour, E., & Forestini, M. 2000, *A&A*, 358, 593
- Skrutskie, M. F., Cutri, R. M., Stiening, R., et al. 2006, *AJ*, 131, 1163
- Slesnick, C. L., Carpenter, J. M., Hillenbrand, L. A., & Mamajek, E. E. 2006, *AJ*, 132, 2665
- Slettebak, A. 1955, *ApJ*, 121, 653
- Smith, A. M. S., & WASP Consortium. 2014, *Contributions of the Astronomical Observatory Skalnaté Pleso*, 43, 500
- Song, I., Zuckerman, B., & Bessell, M. S. 2012, *AJ*, 144, 8
- Spencer Jones, H., & Jackson, J. 1936, *Proper Motions of Stars in the Zone Catalogue -40 to -52 degrees of 20843 Stars for 1900*
- Struve, O., & Straka, W. C. 1962, *PASP*, 74, 474
- Stfan van der Walt, S. C. C., & Varoquaux, G. 2011, *The NumPy Array: A Structure for Efficient Numerical Computation*, . <http://www.scipy.org/>
- Torres, C. A. O., Quast, G. R., da Silva, L., et al. 2006, *A&A*, 460, 695
- van Leeuwen, F., ed. 2007, *Astrophysics and Space Science Library, Vol. 350, Hipparcos, the New Reduction of the Raw Data*
- Vrba, F. J., Strom, S. E., & Strom, K. M. 1976, *AJ*, 81, 958
- Watson, C. L. 2006, *Society for Astronomical Sciences Annual Symposium*, 25, 47
- Wichmann, R., Sterzik, M., Krautter, J., Metanomski, A., & Voges, W. 1997, *A&A*, 326, 211

APPENDIX

A. PERIODS FOR OTHER STARS IN SCO-CEN COMPLEX

SuperWASP time series photometry was found for 27 other stars. These stars are associated with neighboring subgroups (some of which are active star-forming regions, e.g. Lup, Oph, CrA), i.e. their positions and/or kinematics are inconsistent with membership within the three classic older subgroups (LCC, UCL, US). Two are associated with the TW Hya group. We also found a Li-rich K giant with two measured periods, which is elaborated on later in the appendix. Their estimated rotation periods (calculated following the analysis in §3), along with their 2MASS alias and spectral type are presented in Table 3.

B. A MASSIVE ECLIPSING BINARY IN OPHIUCHUS: V2394 OPH

1SWASP J163140.67-242516.2 (V2394 Oph, TYC 6799-309-1, CoD-24 12698) is a 0.59 day eclipsing binary whose components are probably either in contact or close. The star is situated in the LDN 1689 cloud (Nutter et al. 2006), and has been previously selected as a proper motion member of either Upper Sco (Hoogerwerf et al. 2000) and/or Oph (Makarov 2007). A very strong period of 0.295 day is clearly detected in all three seasons of SuperWASP data. Phase-folded time series photometry at 0.295 day suggests that the secondary eclipse depth is ~ 0.2 mag and the primary eclipse depth is ~ 0.4 mag. The long-term out-of-eclipse brightness seems to be varying at the ~ 0.1 mag level over the three years. Grankin et al. (1996) report the eclipsing binary to have photometry at maximum of $V = 10.01$, $U - B = 0.40$, $B - V = 0.95$. Barnard (1910) and Struve & Straka (1962) both commented on the concentration of nebulosity centered on the star (called CD -24° 12684 in these publications), and Struve & Straka (1962) comments on a very red *reflection nebula* surrounding the star and reports that a spectrum taken by George Herbig in 1949 revealed the star to be A0 or A1. Vrba et al. (1976) reported the star (VSS II-50) as spectral type B9, and estimated the star to have extinction $A_V \simeq 3.29$ ($E(B - V) = 1.06$). The Grankin et al. (1996) colors at maximum light are a good match to a $T_{\text{eff}} \simeq 9700$ K dwarf with $E(B - V) = 1.47$ ($A_V = 4.87$ mag), which would be consistent with \sim A0 type.

Is this star associated with Sco-Cen? The Gaia DR1 TGAS astrometry for star lists proper motion $\mu_\alpha, \mu_\delta = -6.672, -24.594$ ($\pm 1.599, \pm 1.803$) mas yr^{-1} and parallax $\varpi = 7.23 \pm 0.58$ mas (consistent with distance 138 ± 11 pc). The proper motion is similar to the mean proper motion of the YSOs in the Oph embedded cluster: $\mu_\alpha, \mu_\delta = -10, -27$ ($\pm 2, \pm 2$) mas yr^{-1} (Mamajek 2008). The mean distance to the Oph cluster has been estimated recently to be 131 ± 3 pc (Mamajek & Hillenbrand 2008), 119 ± 6 pc (Lombardi et al. 2008), $120.0^{+4.5}_{-4.2}$ pc (Loinard et al. 2008), but a recent VLBA trigonometric parallax survey of 16 systems by Ortiz-León et al. (2016) refined the mean distance to 137.3 ± 1.2 pc. Hence, both the Gaia DR1 TGAS proper motion and parallax are statistically consistent with the rest of the YSO population in the Oph cloud. If the star is associated with Oph, its radial velocity is predicted to be -6.5 km s^{-1} . The star is in very close proximity with 4 other lower-mass YSOs within $3'$ (~ 0.12 pc projected radius; DoAr 43, 44, 46, and 2MASS J16313124-2426281), which may consist of an unstable dynamical trapezium.

Hence, V2394 Oph appears to be not only comoving with Upper Sco and Oph, in the immediate vicinity of other YSOs, associated with nebulosity, and a Gaia DR1 parallax consistent with being co-distant with the Oph clouds (see clumping of parallaxes for stars illuminating reflection nebulae in Mamajek & Hillenbrand 2008). The photometry is consistent with an unresolved, unextincted V_o magnitude of 5.14. Using the TGAS parallax, we estimate an unresolved absolute magnitude of $M_V = -0.6$, which places it about 2 mag above the zero-age main sequence (Aller et al. 1982). Through comparison with the Siess et al. (2000) isochrones, and considering the unknown mass and radii ratios of the components, we propose that the V2364 Oph system is a ~ 1 -2 Myr-old contact or near-contact eclipsing binary where the primary is a ~ 3 -5 M_\odot star. Erickson et al. (2011) only identify four members of the Oph clouds whose spectral types are A0 or earlier (HD 147889, SR 3, Oph S1, WLY 2-48), and now V2394 Oph appears to be the most massive member specifically of the LDN 1689 dark cloud.

C. OTHER ECLIPSING BINARIES

1SWASP J140807.34-393548.8 (TYC 7807-358-1, ASAS J140807-3935.9, CD-39 8717) appears to be a 7.815 day eclipsing binary with primary eclipse depth of ~ 0.7 mag and secondary eclipse depth of ~ 0.6 mag. The strongest peaks have periods of 7.83 days (the season 1 phase-folded light curve shows two minima), 3.91 days (the season 2 single minimum), and 3.895 days (the season 3 single minimum with large scatter). This star was selected as a candidate UCL member by virtue of its proper motion by Hoogerwerf et al. (2000). The UCAC4 proper motion is suggestive of LCC membership, however the kinematic parallax ($\varpi = 9.30 \pm 0.62$ mas) we calculate using the UCAC4

proper motion and LCC space motion from [Chen et al. \(2011\)](#) differs from the Gaia DR1 parallax ($\varpi = 2.98 \pm 0.75$ mas) by 6.5σ . We conclude that this is a background interloper unrelated to Sco-Cen.

1SWASP J151126.76-361457.2 (HD 134518) is a 1.154 day eclipsing binary with a primary eclipse depth of ~ 0.15 mag and secondary eclipse depth of ~ 0.05 mag. Very strong peaks at exactly 0.577 days are detected in each of the three seasons. This star was mentioned as a UCL candidate by [de Geus et al. \(1989\)](#). [Perevozkina & Svechnikov \(2004\)](#) classifies the system as A7+[K5], and [Houk \(1982\)](#) classifies the blended spectrum as A8V. The revised Hipparcos parallax ($\varpi = 7.72 \pm 1.81$ mas [van Leeuwen 2007](#)) and light estimated reddening ($E(B-V) \simeq 0.09$) are both similar to other UCL members (mean $\varpi \simeq 7.1$ mas), however the revised Hipparcos proper motion is off of the mean UCL motion ([Chen et al. 2011](#)) by $\sim 5 \text{ km s}^{-1}$ - much larger than the 1D velocity dispersion of the group ($\sim 1.3 \text{ km s}^{-1}$). The Hipparcos parallax translates the primary's HRD position to on the main sequence and below the trend for other Sco-Cen members. We consider HD 134518's membership to UCL unlikely, but further follow up is warranted. If HD 134518 belongs to UCL, its systemic radial velocity should be 3 km s^{-1} .

1SWASP J153554.13-335623.6 (TYC 7322-822-1) is a 1.06 day eclipsing binary showing a primary eclipse depth of ~ 0.3 mag and secondary eclipse depth of ~ 0.2 mag. The system showed very clean 0.53 day peaks in all three seasons. [Hoogerwerf et al. \(2000\)](#) selected the star as a candidate UCL member based on its proper motion. The star's Gaia DR1 parallax ($\varpi = 3.19 \pm 0.78$ mas) differs from the kinematic parallax we calculate ($\varpi = 8.52 \pm 0.70$ mas; adopting its UCAC4 proper motion and assuming UCL space velocity from [Chen et al. 2011](#)) by 5.1σ . We conclude that this is a background interloper.

1SWASP J154856.93-363920.2 (TYC 7340-720-1) is a 0.393 day contact binary with primary eclipse depth of ~ 0.10 mag and secondary eclipse depth of ~ 0.08 mag. [Hoogerwerf et al. \(2000\)](#) selected this star as a candidate UCL member based on its proper motion. The Gaia DR1 parallax ($\varpi = 6.51 \pm 0.32$ mas) is similar to other UCL members, however the Gaia TGAS proper motion is off of the predicted UCL motion by $8 \pm 1 \text{ mas yr}^{-1}$ ($7 \pm 1 \text{ km s}^{-1}$). We conclude that the star is an interloper.

D. A LI-RICH RED GIANT INTERLOPER

1SWASP J111434.43-441824.1 (2MASS J11143442-4418240, CD-43 6891) gave conflicting signals regarding its potential Sco-Cen membership. The star was found by [Pecaut & Mamajek \(2016\)](#) to be a Li-rich (EW(Li I $\lambda 6707$) = 670 m\AA) X-ray-emitting K2IV star, however its inferred isochronal age (1 Myr) appeared to be extraordinarily young. The star has a large photometric amplitude (~ 0.2 mag) and long period (37 day), for which [Richards et al. \(2012\)](#) classified its light curve as that of a small-amplitude red giant type B. Both [Rybka \(2007\)](#) and [Gontcharov \(2008\)](#) flag the star as being a likely clump red giant. The new Gaia DR1 parallax ($\varpi = 2.18 \pm 0.25$ mas; [Gaia Collaboration et al. 2016](#)) is clearly at odds with the predicted kinematic parallax calculated by [Pecaut & Mamajek \(2016, ; \$\varpi = 6.56 \pm 0.60\$ mas; which assumed Sco-Cen membership\)](#). Ignoring the effects of extinction, this translates to an absolute magnitude of $M_V \simeq 1.5$, which puts it squarely among other K2 giants. We conclude that the star is a rare Li-rich giant, and an interloper.

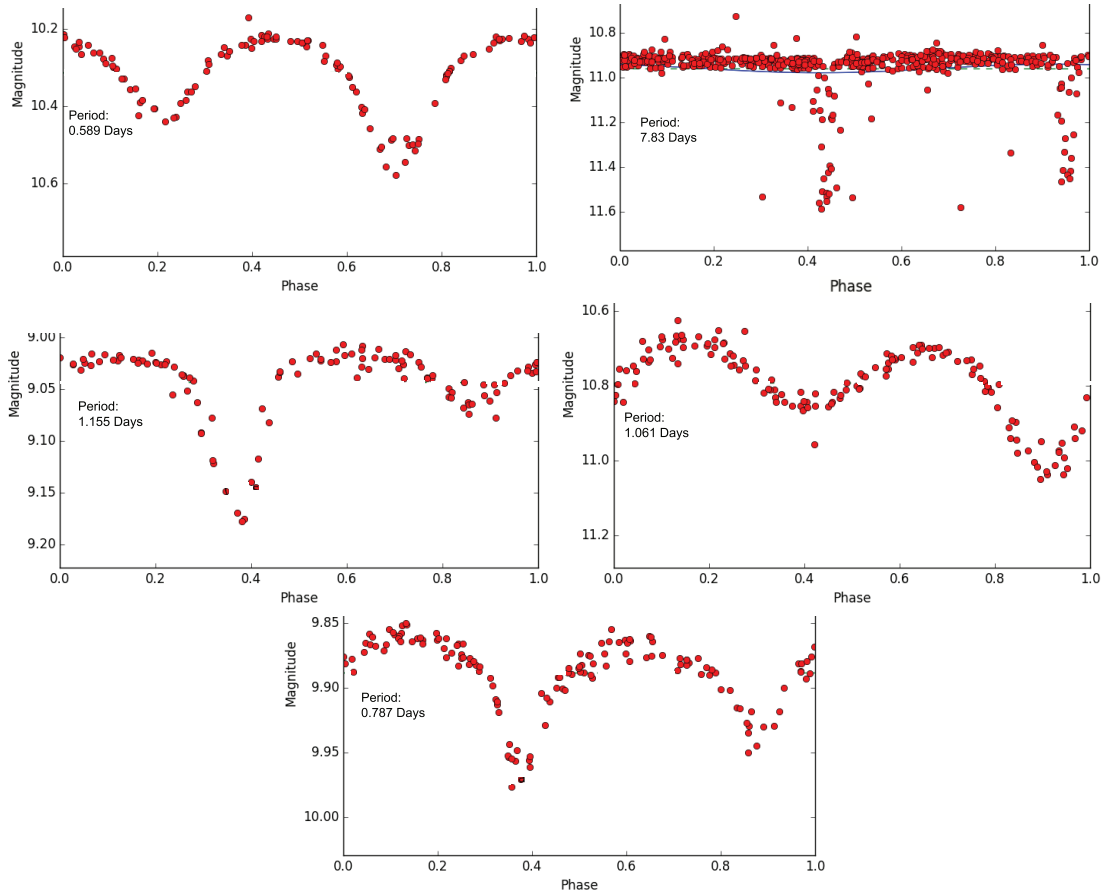


Figure 9. Phase-folded light curves for our five eclipsing binary detections (all season 1 detections). *Top Left:* TYC 6799-309-1, *Top Right:* TYC 7807-358-1, *Middle Left:* HD 134518, *Middle Right:* TYC 7322-822-1, *Bottom:* TYC 7340-720-1.

Table 1. Periodogram Analysis Results

1SWASP (J)	Season Start (HJD)	Season End (HJD)	Period (Days)	Amplitude (Mag)
111327.46-452332.7	2453860.2218	2453924.2104	0.628	0.038
111327.46-452332.7	2454105.5074	2454307.2128	0.628	0.035
111327.46-452332.7	2454467.4436	2454614.2497	0.628	0.039
111434.43-441824.1	2453860.2219	2453924.2103	0.974	0.067

NOTE—This table contains all of the rotation period information extracted from the complete 1689 star sample. The remainder of the table is available electronically. Each entry is for one SWASP object for a single season between the reported HJD dates. For each season, we report the identifiers, season HJDs, strongest period(s) in that season, and the amplitude of the phase-folded light curve.

Table 2. Data for Sco-Cen Members

1SWASP (J)	2MASS (J)	Subgroup ...	Period (days)	SpT ...	Ref. ...	V (mag)	K_S (mag)	A_V (mag)	$(V - K_S)_0$ (mag)	T_{eff} (K)	M/M_\odot ...
111327.46-452332.7	11132622-4523427	LCC	0.628 ± 0.002^a	M0.5	1	12.83	8.50	0.278	4.090	3700	0.56
112102.95-462630.9	11210295-4626308	LCC	3.798 ± 0.844^a	–	–	11.09	8.96	0.194 ^c	1.935	–	–
114445.40-455106.2	11444540-4551062	LCC	2.166 ± 0.016	–	–	9.94	8.57	0.194 ^c	1.174	–	–
124419.32-452523.3	12441932-4525235	LCC	3.122 ± 0.044	F9V	3	9.60	8.00	0.279	1.350	6090	1.35

NOTE— This table contains the members of Sco-Cen reported based on the criteria described in §3.1.2. The remainder of the table is available electronically. Provided are cross-identifications of SWASP and 2MASS identifiers, periods and uncertainties, the spectral type and reference for the 157 stars with spectral types, APASS V magnitudes, 2MASS $V - K_s$ magnitudes, adopted reddening coefficients, T_{eff} , and mass.

(^a) Stars which have statistically similar periods to the nearest spatial entry in the Variable Star Index (Watson 2006).

(^b) Stars which have statistically different periods to the nearest spatial entry in the Variable Star Index (Watson 2006).

(^c) Stars without spectral types use the Sco-Cen sub-group-averaged reddening coefficients for color estimation only.

(^d) The only star in our sample found in David et al. (2014). We find the same period.

(^e) Stars for which APASS V band was unavailable; SPM4 photometry was adopted in its place.

References: (1) Riaz et al. (2006), (2) Pecaut & Mamajek (2016), (3) Houk (1978), (4) Mamajek et al. (2002), (5) Spencer Jones & Jackson (1936), (6) Torres et al. (2006), (7) Houk (1982), (8) Wichmann et al. (1997), (9) Krautter et al. (1997), (10) Köhler et al. (2000), (11) Preibisch et al. (1998), (12) Houk & Smith-Moore (1988), (13) Rizzuto et al. (2015), and (14) Luhman & Mamajek (2012).

Table 3. Data for Other Stars

Name	Group	1SWASP (J)	2MASS (J)	Period (days)	Spectral Types	Ref.
CD-43 6891	...	111434.43-441824.1	11143442-4418240	0.973 ± 0.004^b	K2IV	5
CD-43 6891	...	111434.43-441824.1	11143442-4418240	39.92 ± 2.10^a	K2IV	5
TWA 12	TWA	112105.46-384516.5	11210549-3845163	3.311 ± 0.051^a	M1Ve	1
TWA 20	TWA	123138.06-455859.3	12313807-4558593	1.822 ± 0.014^a	M3IVe	5
RX J1539.7-3450	Lup I	153946.41-345102.2	15394637-3451027	7.127 ± 0.204^a	K4	2
HT Lup	Lup I	154512.86-341730.5	15451286-3417305	4.304 ± 0.109^a	K3Ve	1
HD 140655	Lup I	154558.54-341341.2	15455855-3413411	2.753 ± 0.035	F8V	3
RX J1546.8-3459	Lup I	154645.09-345947.3	15464506-3459473	2.278 ± 0.025	M0	2
RX J1548.1-3452	Lup I	154808.93-345253.2	15480893-3452531	1.423 ± 0.020	M2.5	2
RX J1548.9-3513	Lup I	154854.16-351318.5	15485411-3513186	0.933 ± 0.003	K6	2
IM Lup	Lup II	155609.20-375605.9	15560921-3756057	7.309 ± 0.183	M0	4
MML 78	Lup III	160545.00-390606.5	16054499-3906065	1.261 ± 0.007^a	G7V	5
RX J1607.2-3839	Lup III	160713.73-383923.3	16071370-3839238	2.418 ± 0.026	K7	2
IRAS 16051-3820	Lup III	160830.70-382826.8	16083070-3828268	6.244 ± 0.129	K0?	6
RX J1608.9-3905	Lup III	160854.27-390605.6	16085427-3906057	2.005 ± 0.028^a	K2	2
V1095 Sco	Lup III	160939.52-385506.8	16093953-3855070	2.912 ± 0.037^a	K5	2
Sz 122	Lup III	161016.43-390805.0	16101642-3908050	0.287 ± 0.001	M2e	4
RX J1612.0-3840	Lup III	161201.38-384027.5	16120140-3840276	2.813 ± 0.033^a	K5	2
RX J1620.7-2348	Oph	162045.96-234820.2	16204596-2348208	3.355 ± 0.139	K3e	7
RX J1621.0-2352	Oph	162057.86-235234.4	16205787-2352343	2.097 ± 0.046^a	G9IV	1
EM* StHa 126	Oph	162307.84-230059.8	16230783-2300596	4.069 ± 0.235^a	K2	7
EM* SR 6	Oph	162528.63-234626.1	16252863-2346265	3.760 ± 0.119	K2IV	5
CD-27 10938	Oph	162627.35-275651.0	16262736-2756508	2.065 ± 0.281^a	K4IVe	5
VSS II-28	Oph	162652.81-234312.6	16265280-2343127	5.595 ± 0.322^a	K1IVe	5
HBC 644	Oph	163104.44-240435.8	16310436-2404330	0.973 ± 0.019^b	K4IVe	5
V940 Sco	Oph	163201.59-253025.7	16320160-2530253	2.452 ± 0.035^a	K5IVe	5
V709 CrA	CrA	190134.84-370056.6	19013485-3700565	2.244 ± 0.021	K2.5	8
RX J1917.4-3756	CrA	191723.82-375650.3	19172382-3756504	3.375 ± 0.045^a	K0IVe	1

NOTE—^(a) Stars which have statistically similar periods to the nearest spatial entry in the Variable Star Index (Watson 2006).

^(b) Stars which have statistically different periods to the nearest spatial entry in the Variable Star Index (Watson 2006).

References: (1) Torres et al. (2006), (2) Krautter et al. (1997), (3) Houk (1982), (4) Hughes et al. (1994), (5) Pecaut & Mamajek (2016) (6) Antonucci et al. (2014) (estimates $T_{\text{eff}} = 5000$ K, which would be roughly consistent with a K0 pre-MS star on the spectral type vs. T_{eff} scale of Pecaut & Mamajek (2013)), (7) Preibisch et al. (1998), (8) Meyer & Wilking (2009).

Table 4. Adopted Photometry For Stellar Parameters

2MASS (J)	B (mag)	Ref.	V (mag)	Ref.	J (mag)	H (mag)	K_S (mag)
11132622-4523427	14.370±0.012	DR9	12.833±0.010	DR9	9.415±0.028	8.727±0.040	8.495±0.031
12441932-4525235	10.087±0.035	H00	9.500±0.022	H00	8.371±0.027	8.072±0.047	7.999±0.033
12480778-4439167	10.650±0.014	T06	9.830±0.010	T06	8.131±0.021	7.672±0.055	7.513±0.024
12543141-4607361	10.250±0.038	H00	9.713±0.024	H00	8.376±0.029	7.983±0.024	7.910±0.023

NOTE—A sample of the adopted photometry for the stars with spectral types. The remainder of this table is available electronically. AAVSO Photometric All-Sky Survey (APASS) DR6, DR7 photometry retrieved from <https://www.aavso.org/download-apass-data>; Henden et al. (2016).
References – (DR6) APASS DR6; (DR7) APASS DR7; (DR9) APASS DR9; (P97) Hipparcos, Perryman et al. (1997); (H00) Converted from Tycho-2 B_T , V_T , Høg et al. (2000); (T06) Torres et al. (2006).